9190 *Biochemistry* **2010,** *49,* 9190–9198
DOI: 10.1021/bi1013722

BIOCHEMISTRY
including biophysical chemistry & molecular biology
Article

Lipid−Protein Correlations in Nanoscale Phospholipid Bilayers Determined by Solid-State Nuclear Magnetic Resonance[†]

Aleksandra Kijac,[‡] Amy Y. Shih,[§] Andrew J. Nieuwkoop,[∥] Klaus Schulten,[‡,§,∥] Stephen G. Sligar,[‡,§,∥,⊥] and Chad M. Rienstra*[,‡,§,∥]

[‡]*Center for Biophysics and Computational Biology,* [§]*Beckman Institute for Advanced Science and Engineering,* [∥]*Department of Chemistry, and* [⊥]*Department of Biochemistry, University of Illinois, Urbana, Illinois 61801*

Received August 25, 2010; Revised Manuscript Received August 29, 2010

ABSTRACT: Nanodiscs are examples of discoidal nanoscale lipid−protein particles that have been extremely useful for the biochemical and biophysical characterization of membrane proteins. They are discoidal lipid bilayer fragments encircled and stabilized by two amphipathic helical proteins named membrane scaffolding protein (MSP), ∼10 nm in size. Nanodiscs are homogeneous, easily prepared with reproducible success, amenable to preparations with a variety of lipids, and stable over a range of temperatures. Here we present solid-state nuclear magnetic resonance (SSNMR) studies on lyophilized, rehydrated POPC Nanodiscs prepared with uniformly ^{13}C-, ^{15}N-labeled MSP1D1 (Δ1−11 truncated MSP). Under these conditions, by SSNMR we directly determine the gel-to-liquid crystal lipid phase transition to be at 3 ± 2 °C. Above this phase transition, the lipid ^{1}H signals have slow transverse relaxation, enabling filtering experiments as previously demonstrated for lipid vesicles. We incorporate this approach into two- and three-dimensional heteronuclear SSNMR experiments to examine the MSP1D1 residues interfacing with the lipid bilayer. These ^{1}H−^{13}C and ^{1}H−^{13}C−^{13}C correlation spectra are used to identify and quantify the number of lipid-correlated and solvent-exposed residues by amino acid type, which furthermore is compared with molecular dynamics studies of MSP1D1 in Nanodiscs. This study demonstrates the utility of SSNMR experiments with Nanodiscs for examining lipid−protein interfaces and has important applications for future structural studies of membrane proteins in physiologically relevant formulations.

The structure and function of membrane proteins are often significantly affected by the specific properties of the lipid bilayer in which the protein is embedded or tethered. A number of membrane bilayer properties such as cholesterol content, lipid headgroup charge, saturation of the lipid acyl chains, and length of the acyl chains can be crucial for proper folding and function of the membrane protein. Given that the native membrane itself can be closely tied to structural and functional properties of a membrane protein, comprehensive studies of membrane proteins should consider the structure and function of these proteins in the context of the native membrane environment and appropriate lipid components. Examples of effects of a membrane on protein structure and/or function can be found in proteins involved in the blood coagulation cascade (*1*, *2*), drug-metabolizing cytochrome P450s (*3*−*5*), G-protein-coupled receptors (GPCRs) (*6*), ion channels (*7*, *8*), and antimicrobial peptides (*9*−*11*). The constitution of lipid membranes can affect the binding affinity between proteins, catalytic efficiency, and enzymatic activity of a membrane protein (*3*, *7*, *12*). The interaction between membrane proteins and the membrane bilayer implies that structural and functional studies of membrane proteins should take all necessary precautions in the preparation of protein−bilayer mimetic assemblies and ensure that the chosen conditions do not alter the protein's native structure or function, which often represents a challenging prospect (*13*, *14*).

In the past decade, a new membrane mimetic has been developed and well characterized for structural and functional studies of membrane proteins (*15*−*23*). This mimetic, called the Nanodisc (Figure 1a), consists of a ∼10 nm discoidal lipid bilayer encircled and stabilized by two molecules of amphipathic helical membrane scaffolding protein (MSP),[1] derived from nascent high-density lipoproteins (HDLs) (*16*). Studies of Nanodiscs have been important in improving our understanding of many aspects of self-assembly and properties of HDLs (*19*, *20*, *24*, *25*). More importantly, Nanodiscs have been instrumental in a number of functional and structural studies on various membrane proteins, including rhodopsin and bacteriorhodopsin (*21*, *23*), cytochrome P450s (*17*, *26*−*28*), tissue factor (*2*), and others (*29*−*31*). To facilitate structural analysis of MSP, the protein component of Nanodiscs, we have developed methods for the preparation of Nanodiscs for SSNMR studies (*32*). We have further shown that membrane proteins can be assembled in Nanodiscs and prepared in an active state suitable for

[†]This work was supported by National Institutes of Health Grants GM33775 and GM31756 (to S.G.S.), GM79530 (to C.M.R. and M. A. Schuler), and R01-GM067887 and P41-RR05969 (to K.S.) and Grant MCB 0234938 (to K.S.) from the National Science Foundation. A.Y.S. acknowledges support from a Beckman Postdoctoral Fellowship.

*To whom correspondence should be addressed. Phone: (217) 244-4655. Fax: (217) 244-3186. E-mail: rienstra@scs.uiuc.edu.

[1]Abbreviations: CP, cross-polarization; DMPC, 1,2-dimyristoyl-*sn*-glycero-3-phosphocholine; DPPC, 1,2-dipalmitoyl-*sn*-glycero-3-phosphocholine; DSC, differential scanning calorimetry; MAS, magic-angle spinning; MD, molecular dynamics; MSP, membrane scaffolding protein; MSP1D1, Δ1−11 truncated membrane scaffolding protein; PEG, polyethylene glycol; POPC, 1-palmitoyl-2-oleoylphosphatidylcholine; SPC5, Supercycled POST-C5; SSNMR, solid-state nuclear magnetic resonance; TPPM, two-pulse phase modulation.

 Published on Web 08/30/2010

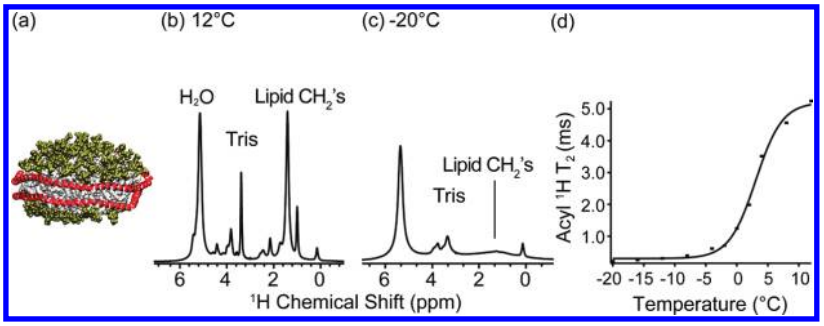

FIGURE 1: Gel to liquid crystalline transition of lipids in Nanodiscs. (a) Cartoon representation of a Nanodisc with MSP1D1 colored red, POPC headgroups green, and tails white. 1D ^{1}H spectra of POPC Nanodiscs at (b) 12 and (c) −20 °C. Spectra were recorded on a 600 MHz (^{1}H frequency) spectrometer. The acyl ^{1}H line width and peak height indicate the phase transition. (d) Graph of T_2 values as a function of temperature for the acyl methylene ^{1}H signals (1.3 ppm). The lipid phase transition in POPC Nanodiscs is determined to be at 3 °C.

SSNMR (*33*). Recently, Nanodiscs have also been used to successfully study peptides and even integral membrane proteins using solution NMR (*34*−*36*). Depending on the membrane protein of interest, Nanodiscs can offer a number of advantages over other traditionally used membrane mimetics. They can be assembled with a variety of lipids and lipid mixtures, allowing for precise control of the lipid composition in the microenvironment of the embedded protein (*16*, *27*, *37*). This proved to be quite useful in the studies of blood clotting, where the use of Nanodiscs gave insights into the effects of an increasing amount of charged phospholipids in the bilayer and that of a bilayer made completely of charged phospholipids on the activity of the proteins involved in the initiation of the blood clotting cascade (*12*, *38*). Nanodiscs also provide access to both sides of the embedded transmembrane proteins and allow control of the oligomeric state of the incorporated protein (*17*, *21*), which is quite difficult in detergent micelles or liposomes. This has previously allowed investigations into the functional properties of a monomeric human drug-metabolizing protein cytochrome P450 3A4 (*39*, *40*), whose function has been known to be affected by its aggregation state (*41*), impossible to control in other membrane mimetics. Nanodiscs have also allowed functional assessments and comparisons between monomeric and oligomeric protein assemblies in the case of seven-transmembrane proteins (*42*, *43*), the bacterial chemoreceptor (*37*), and the peptide translocon complex (*44*, *45*). In addition, Nanodiscs are amendable to incorporation of well-defined protein assemblies, and studies of a single P450 enzyme complexed with its redox partner in a Nanodisc have provided valuable insights (*39*, *46*, *47*). Reviews of Nanodiscs as well as numerous membrane proteins studies that have benefited from the use of Nanodiscs have recently been published (*48*, *49*). Advantages provided by the Nanodisc system allow one to probe changes in protein conformation, protein−membrane interfaces, and the depth of membrane insertion as a function of lipid composition. The combination of these advantages and the stability of Nanodiscs under SSNMR experimental conditions make Nanodiscs a promising platform for structural studies of membrane proteins in their native membrane environment using SSNMR.

SSNMR has been extensively applied in the recent years to structural studies of membrane proteins (*50*−*53*), fibrils (*54*−*56*), and other supramolecular assemblies that remained inaccessible to other biophysical techniques. In particular, SSNMR is a powerful tool for obtaining detailed information about the membrane−protein interface and can yield information about the assembly of membrane proteins into functional oligomeric complexes, orientation (*57*−*59*), dynamics, location, and depth of insertion of proteins in the membrane (*60*−*66*), as recently reviewed (*67*).

In this study, we use two-dimensional (2D) and three-dimensional (3D) magic-angle spinning (MAS) SSNMR to investigate lipid−protein interfaces using the Nanodisc platform. Our experiments use proton spin diffusion, where magnetization from a spin source is selected on the basis of mobility and transferred to the target protein. In this particular case, lipids are the spin source, because they are mobile and have relatively long T_2 relaxation times (several milliseconds or more, depending on temperature) above the lipid phase transition. Our studies are modeled after similar studies in which lipids within vesicles were used as the magnetization source (*64*), but complementary information with water as the magnetization source can be obtained with proteins embedded in the bilayer below the lipid phase transition temperature (*68*). In either case, a ^{1}H T_2 filter is used to select for the mobile ^{1}H spins, and the ^{1}H signals from the relatively rigid protein are suppressed by this filter. In the studies in which lipid protons are the source of magnetization, the spin diffusion from lipid protons is fast for the transmembrane domains of a protein, while this is not the case for proteins with domains residing at the bilayer−water interface.

Here we use these proton spin diffusion experiments to examine the lipid−protein interface of MSP in a Nanodisc. We describe a new method of preparation of Nanodisc samples for SSNMR that is compatible with the more physiologically relevant POPC lipids. Studies presented here demonstrate that Nanodiscs retain the phase transition behavior of lipid bilayers in biological membranes under SSNMR sample preparation conditions, and that the lipid:protein ratio is sufficiently low (i.e., sample sensitivity high) to yield three-dimensional ^{1}H−^{13}C−^{13}C spectra of MSP. The experimental spectra are compared to the molecular dynamic (MD) simulation results for MSP. The SSNMR spectra of MSP allow for amino acid type assignments, and the quantification of the 2D and 3D spectra by amino acid type is consistent with the results of MD simulations. This work shows the potential of combining SSNMR with the Nanodisc platform for the examination of membrane protein topology and protein−membrane interfaces.

EXPERIMENTAL PROCEDURES

Sample Preparation. Nanodiscs were made with uniformly ^{13}C-, ^{15}N-labeled MSP1D1 (a Δ1−11 truncation construct of MSP1, shown to form more stable Nanodiscs) (*18*) and 1-palmitoyl-2-oleoylphosphatidylcholine (POPC) lipids, and the SSNMR sample was lyophilized and rehydrated. Uniformly ^{13}C-, ^{15}N-labeled MSP1D1 was expressed in *Escherichia coli*

following a protocol described previously (*32*) and purified using Chelating Sepharose Fast Flow (Amersham Biosciences, Piscataway, NJ) charged with Ni^{2+} according to the manufacturer's instruction, and a seven-His tag on the scaffolding protein. The expression protocol yields ~20 mg of isotopically labeled MSP1D1 per liter of growth medium. The preparation of empty Nanodiscs was performed as described previously (*16*), using POPC lipids (Avanti Polar Lipids, Alabaster, AL). In short, lipids from a chloroform stock were dried under a stream of nitrogen gas and left in vacuo overnight for the removal of residual chloroform. They were subsequently solubilized in a sodium cholate-containing buffer [10 mM Tris-HCl and 0.1 M NaCl (pH 7.4)] where the lipid:cholate ratio was 1:2 and the lipid concentration was approximately 50 mM. Incubation of the mixture in warm water and subsequent sonication results in complete solubilization of the lipids. MSP1D1 was then added to this mixture in a 1:65 ratio with POPC lipids (*16*). This mixture was incubated for approximately 1 h at 4 °C. Finally, the self-assembly was initiated by removal of detergent during incubation with hydrophobic Amberlite XAD2 beads (Supelco, Bellefonte, PA) for 4−5 h at 4 °C with moderate agitation. The final step of Nanodisc preparation was gel permeation chromatography, performed on a Superdex 200 HR 10/30 column (Amersham Biosciences) using a Waters Millenium HPLC system with a diode array detection system. The column was equilibrated in buffer [10 mM Tris-HCl and 100 mM NaCl (pH 7.4)]. The mobile phase flow rate was 0.5 mL/min, with monitoring of the protein absorbance at 280 nm, and one fraction collected per minute. Gel permeation chromatography can also be used to test the stability of the sample after experimental manipulations.

After being purified, Nanodiscs were exchanged into a 40 mM Tris-HCl, 10 mM NaCl (pH 7.4) buffer and concentrated to approximately 300 μM using an Amicon ultra centrifugal filter unit with a molecular weight cutoff of 10000 (Millipore, Billerica, MA). This ensured that the NaCl concentration would remain low in the lyophilized pellet. Trehalose was added in a 1:1 (w/w) ratio with the lipid as a lyoprotectant. The sample was then flash-frozen in liquid nitrogen and lyophilized overnight. The stability of POPC Nanodiscs under this lyophilization procedure was tested by resuspension of the samples in water and examination by size exclusion chromatography.

The uniformly ^{13}C-, ^{15}N-labeled MSP1D1 POPC Nanodisc sample was transferred to a 3.2 mm thin wall rotor (Varian NMR, Palo Alto, CA) with a working volume of ~36 μL and confined to the active sample region of the rotor by Kel-F and rubber spacers as described elsewhere (*69*). The mass of MSP1D1 in the rotor was determined to be ~4 mg by comparison of the intensity of one-dimensional (1D) ^{13}C spectra to standard proteins with known quantities. The mass of lipids, based upon the stoichiometry of the Nanodisc, was estimated to be ~10 mg, and the mass of trehalose was ~10 mg. This material was directly rehydrated in the SSNMR rotor with 10 μL of water, which was determined to be sufficient for the observation of a bulk H_2O signal at ~5 ppm in the 1D ^1H spectrum.

SSNMR Spectroscopy. All SSNMR experiments were conducted on a 14.1 T (600 MHz ^1H frequency) wide bore magnet with a Varian InfinityPlus NMR spectrometer, equipped with a 3.2 mm HXY T3 probe tuned in $^1H-^{13}C-^{15}N$ mode. Spectra were recorded at a magic-angle spinning (MAS) rate of 10 kHz. Pulse sequences were implemented with tangent-ramped cross-polarization (CP) (*70*) with two-pulse phase modulation (TPPM) (*71*) ^1H decoupling at ~85 kHz. The typical $\pi/2$ pulse widths were 2.35 μs on ^1H and 2.75 μs on ^{13}C. Data were processed with NMRPipe (*72*) with back linear prediction, and zero filling and Lorentzian-to-Gaussian apodization were employed for each dimension before Fourier transformation. Additional acquisition and processing parameters for each spectrum are included in the figure captions. Chemical shifts were referenced externally to adamantane (*73*).

Molecular Dynamics Simulations of Nanodiscs. Each simulated Nanodisc was comprised of two MSP1D1 proteins and 160 DPPC lipids, and these Nanodiscs were constructed and analyzed using Visual Molecular Dynamics program (VMD) (*74*). The simulation parameters were described in detail elsewhere (*24*).

RESULTS AND DISCUSSION

Sample Preparation. We have shown previously that 1,2-dimyristoyl-*sn*-glycero-3-phosphocholine (DMPC) Nanodiscs can be prepared for SSNMR by precipitation with PEG (*32*). This PEG precipitation procedure cannot be applied to the POPC Nanodiscs, which disassemble under PEG precipitation. The development of new, robust SSNMR sample preparation protocols was necessary for wider application of Nanodiscs, in particular for POPC Nanodiscs because of the greater physiological relevance of POPC lipids and their utility in studying membrane proteins. The lyophilization and rehydration procedure for the preparation of Nanodiscs presented here is simple and highly reproducible and allows ease of sample handling, which includes concentrating Nanodiscs into a very small sample volume without any loss of valuable sample that would occur with the use of common concentrating units. While POPC Nanodiscs can be readily lyophilized from 10 mM Tris-HCl and 100 mM NaCl in the presence of trehalose as a lyoprotectant, this results in a relatively large amount of mobile ions in the rehydrated SSNMR samples. This preparation results in deterioration of the ^1H pulse widths and increased dielectric heating. Although we have previously developed probes that minimize these effects through improved resonator designs (*75*), most commercially available SSNMR probes (including those available for the instruments used in this study) are not designed to perform optimally with samples with an ionic strength of > 50 mM. For SSNMR studies, we desired to decrease the ionic strength for optimal RF probe performance, so we optimized the total ionic strength to address this concern. Therefore, we evaluated the lowest ionic strength that could be achieved while maintaining the integrity of POPC Nanodiscs upon lyophilization.

We found that POPC Nanodiscs are stable under lyophilization in the presence of trehalose if the starting Tris concentration is increased to 40 mM and the NaCl concentration is decreased to 10 mM. After rehydration, these samples exhibit only a small fraction of the detrimental tuning effects of mobile ions in SSNMR, such that T_1 relaxation times of the ^1H signals determined the optimal repetition rate. A size exclusion chromatogram of the resuspended lyophilized Nanodiscs shows that the integrity of Nanodiscs is retained in the process of lyophilization (Figure S1 of the Supporting Information). The integrity of the sample is subsequently monitored by SSNMR spectra.

While Nanodisc samples were fully hydrated during SSNMR experiments, the bulk solution contained a high concentration of trehalose. It is known that sugars do not readily permeate the membrane (*76*); however, it is likely that the OH groups of trehalose form hydrogen bonds with the polar headgroups of the lipid, and in this case with MSP as well, effectively replacing

water molecules. This is known as the water replacement hypothesis (*76*−*78*). However, the results of size exclusion chromatography of lyophilized and rehydrated Nanodisc samples show no increase in size due to specific interactions of trehalose with the Nanodisc (either the bilayer or the MSP), and they indicate that the Nanodisc particles remain intact.

Lipid ^1H 1D Spectra and the Bilayer Phase Transition. As noted in the introductory section, the SSNMR lipid−protein correlation experiments rely on the ability to separate the magnetization from the mobile protons on the lipids or water, relative to protons from the protein. The lipid protons are highly mobile in the liquid crystalline phase. Therefore, it was a prerequisite to examine the behavior of the lipid bilayer in the Nanodisc, as prepared for SSNMR, and confirm that the gel to liquid crystalline phase transition was well-defined, and in agreement with the transition found in lipid bilayers and vesicles. To this end, we performed a series of experiments measuring the ^1H T_2 values of lipids in directly detected ^1H spectra from −20 to 15 °C. [The actual sample temperature for these experiments that, because of frictional and RF heating, varies from the reading on the thermocouple of the probe was calibrated using ethylene glycol (*79*).]

The limiting cases of the liquid crystalline phase (Figure 1b) and the gel phase (Figure 1c) are easily distinguishable in the 1D spectra as monitored by the intensity of the lipid CH_2 and methyl peaks. The transition temperature was fit as the inflection point of the T_2 curve as a function of temperature and thereby determined to be 3 °C (Figure 1d). The relatively narrow (∼0.2 ppm) lipid CH_2 and methyl peaks observed above the lipid phase transition are indicative of the high mobility of lipid acyl chains. Although these T_2 values do not approach values observed for isotropic liquids, they are more than sufficient for the proposed 2D $^1H-^{13}C$ and 3D $^1H-^{13}C-^{13}C$ lipid protein correlation experiments, where ∼1 ms T_2 filters were utilized.

Fully hydrated POPC liposomes undergo gel to liquid crystalline phase transition at approximately −3 °C; dehydrated POPC liposomes undergo the same transition at approximately 60 °C (*78*, *80*), while dehydrated POPC liposomes lyophilized in the presence of trehalose undergo the transition at approximately −20 °C (*78*). The SSNMR-measured phase transition temperature of the lipid bilayer in a Nanodisc of ∼3 °C is certainly consistent with the fully hydrated POPC bilayer in the Nanodisc. This temperature is indeed a few degrees higher than that observed in fully hydrated POPC liposomes; however, this is likely due to the properties of Nanodiscs, rather than the effects of trehalose on the Nanodisc. In support of this, the same phenomenon has been observed in fully hydrated dipalmitoylphosphatidylcholine (DPPC) and dimyristoylphosphatidylcholine (DMPC) Nanodiscs in comparison to DPPC and DMPC liposomes. Previously, the phase transition behavior in Nanodiscs was measured by differential scanning calorimetry (DSC), small angle X-ray scattering (SAXS), and Laurdan fluorescence and showed (for DMPC and DPPC) slightly higher values for the phase transition versus that recorded in vesicles, as well as a relative broadening of this transition (*19*, *20*). The increase in the melting temperature of the lipids in the Nanodiscs is a consequence of additional lateral pressure exerted by the MSP. Namely, the lipid phase transition from the gel to the liquid crystalline phase results in the thermal expansion of the lipid bilayer, which requires an increase in the surface area of the thermodynamically unfavorable lipid−MSP interface, as well as an increase in the size of the MSP belt (*81*). The broadening of the

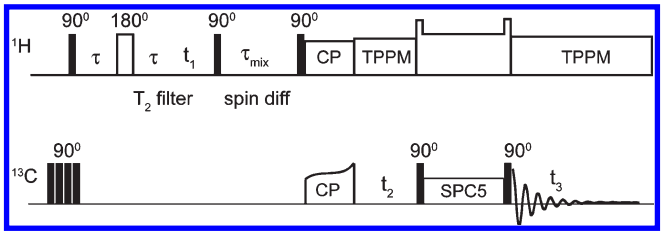

FIGURE 2: $^1H-^{13}C-^{13}C$ 3D pulse sequence used to obtain lipid−protein correlations. Following presaturation of ^{13}C Boltzmann polarization, mobile ^1H signals are selected by a T_2 filter. ^1H polarization is then transferred by spin diffusion to immobile protons, and to the attached ^{13}C by cross-polarization. Following evolution of the ^{13}C chemical shifts, $^{13}C-^{13}C$ mixing is achieved by SPC-5 (*83*), and signals are detected under TPPM decoupling (*71*).

phase transition in Nanodiscs is an established consequence of the size of the lipid bilayer in a Nanodisc, and the relatively small number of lipids participating in the cooperative phase transition. In addition, the boundary lipid associated with the MSP, which constitutes ∼50% of the lipids in these Nanodiscs, is thought to be excluded from the cooperative lipid domain (*81*, *82*).

$^1H-^{13}C-^{13}C$ 3D Spin Diffusion Pulse Sequence with a Double Quantum Filter. To examine the lipid−protein interface, we developed a $^1H-^{13}C-^{13}C$ pulse sequence that takes advantage of the lipid phase transition behavior. Figure 2 shows the 3D ^1H spin diffusion pulse sequence with ^{13}C detection, which we have adapted from earlier versions (*64*) by the addition of an (optional) indirect ^{13}C dimension and double quantum mixing. The four initial 90° pulses on carbon destroy residual ^{13}C magnetization. The ^1H magnetization from the mobile protons (lipids or water) is selected by a T_2 filter after the initial 90° pulse, and frequency labeled in the first dimension. The ^1H signals from the comparatively rigid protein relax during this time because of strong $^1H-^1H$ dipolar couplings, while the lipids have a comparatively long T_2 relaxation time. The 180° pulse in the middle of the filter refocuses the isotropic chemical shift evolution and B_0 field inhomogeneity. The lipid magnetization is then allowed to evolve under the isotropic chemical shift interaction during t_1. A subsequent 90° pulse stores the magnetization along the z-axis and allows magnetization to be exchanged from mobile protons to the (less mobile) protein protons by $^1H-^1H$ spin diffusion during a mixing time τ_{mix}. After this mixing time, another 90° pulse flips the magnetization, which is then transferred to ^{13}C spins via tangent-ramped CP, followed by a ^{13}C evolution period. An SPC-5 mixing period in the $^1H-^{13}C-^{13}C$ 3D experiment is used to observe only one-bond ^{13}C correlations (*83*). The sequence also includes an optional double quantum filter to attenuate the natural-abundance ^{13}C background coming from the large number of natural abundance lipids in the samples. Finally, signals are detected on ^{13}C under TPPM decoupling.

$^1H-^{13}C$ 2D Lipid−MSP Correlations in Nanodiscs. To obtain the $^1H-^{13}C$ 2D correlations of MSP1D1 in a Nanodisc, we first identified and evaluated the strength of the ^{13}C resonances from the natural abundance lipids. To do this, a ^{13}C 1D spectrum was acquired with a 1 ms T_2 filter, without $^1H-^1H$ mixing (Figure 3a). Observed lipid signals are consistent with those previously published belonging to lipid carbons (*9*, *84*). In the ^{13}C 1D spectrum, the strongest lipid signals at ∼32 ppm belong to the CH_2 atoms of the lipid acyl chains. The carbons at the end of the lipid chains (ω) are at ∼18 ppm, followed by ω-1 carbons at ∼23 ppm, and C3 (∼27 ppm), carbons neighboring the oleate double bond carbons (∼29 ppm), and subsequently ω-2 and C2

carbons (~33 and ~35 ppm, respectively). Headgroup carbons (α, β, γ, G1, and G3) are observed between 55 and 70 ppm, and C9 and C10 involved in the double bond are observed at ~130 ppm. Notably, the spectrum observed here arises exclusively from the natural abundance lipids. We also observe individually site-resolved ^{1}H resonances in the ^{1}H−^{13}C 2D correlation spectrum, which are assigned (Figure 3b). The majority of lipid ^{1}H polarization, from the long methylene chain, resides at ~1.3 ppm.

Although the number of ^{13}C sites in the protein is significantly greater than the number of ^{13}C sites in natural abundance lipids, the lipid signals present a potential complication because of their large number (~130 POPC lipids per Nanodisc) and very narrow line widths (~0.2 ppm for ^{13}C). We evaluated the relative intensities by incrementing the ^{1}H−^{1}H spin diffusion time in a series of ^{13}C 1D spectra (Figure 4). The ^{13}C 1D spectrum at very short ^{1}H−^{1}H mixing times (effectively zero mixing, but with the identical phase cycle and number of pulses as subsequent spectra) corresponds to the assigned lipid spectrum in Figure 3a. With an increasing ^{1}H−^{1}H mixing time, in addition to lipid signals, the protein signals are polarized on the time scale of ~30 ms. The protein signal intensity is derived both from the mobile lipid protons and from water, although the latter would have no appreciable contribution to the initial lipid spectrum. At the longer mixing time, the protein signals dominate the total intensity; for example, carbonyl (~175 ppm), Cα (55−65 ppm), aromatic (100−130 and ~160 ppm), Leu Cβ (~40 ppm), and various methyl and methylene ^{13}C sites (15−35 ppm) become prominent in intensity at ~3 ms and dominate the overall spectrum at 30 ms. Nevertheless, sharp lipid peaks are still observed superimposed upon the protein spectrum; this is most readily appreciated by the relative line widths, because the lipids do not experience broadening due to one-bond (residual) ^{13}C−^{13}C dipolar and scalar couplings. Therefore, the intensity of natural abundance lipids would present a challenge in the interpretation of the ^{1}H−^{13}C 2D spectrum of MSP1D1, if superimposed on some protein cross-peaks of significantly lower intensity. Consequently, the ^{1}H−^{13}C 2D sequence implemented on MSP1D1 in Nanodiscs contained a double quantum filter to reduce the ^{13}C background from natural abundance lipids by a factor of 100.

The ^{1}H−^{13}C 2D correlation spectrum of uniformly ^{13}C-, ^{15}N-labeled MSP1D1 in a Nanodisc (Figure 5) contains only water and mobile lipid signals in the ^{1}H dimension, because of the 1 ms T_2 filter. With a 30 ms ^{1}H−^{1}H mixing time, a significant fraction of the polarization is transferred to the protein, as confirmed by the retention of the signal following the double quantum filter. The number of protein resonances correlated to the lipids (~1.3 ppm) and the intensity of lipid−protein cross-peaks are smaller than those of water−protein correlations (at ~5 ppm ^{1}H frequency), which we attribute to the larger initial polarization and longer T_2 for the water resonance. Furthermore, the exposed surface area of the MSP1D1 on the outside of the Nanodisc (exposed to water) is larger than the internal surface area (exposed to lipid). This 1D ^{13}C spectrum has minimal resolution, enabling only a small subset of peaks (e.g., Ala) to be

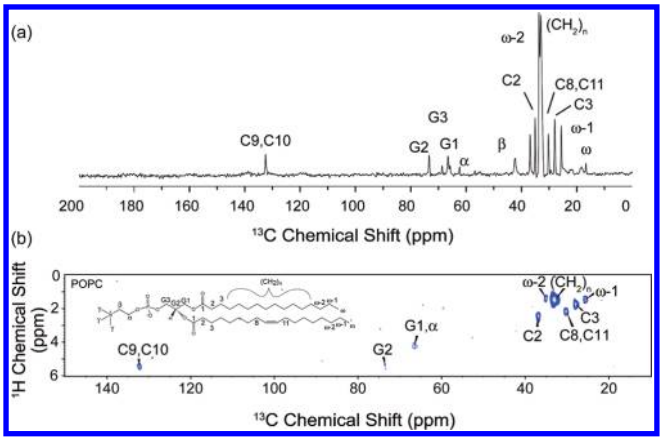

FIGURE 3: ^{13}C 1D and ^{1}H−^{13}C 2D spectra of a POPC bilayer in a Nanodisc. (a) 1D ^{13}C spectrum of Nanodiscs with uniformly ^{13}C-, ^{15}N-labeled MSP1D1 and natural abundance POPC lipids at 8 °C on a 600 MHz (^{1}H frequency) spectrometer. The lipid spectrum was acquired with a 1 ms T_2 filter, no ^{1}H−^{1}H mixing, and a 0.4 ms ^{1}H−^{13}C contact time. The data were processed with 25 Hz Lorentzian-to-Gaussian line broadening. (b) ^{1}H−^{13}C 2D spectrum of the same sample acquired under the same conditions for 6.5 h, with a schematic of a POPC lipid molecule. The spectrum was processed with 100 Hz of Lorentzian-to-Gaussian line broadening in each dimension.

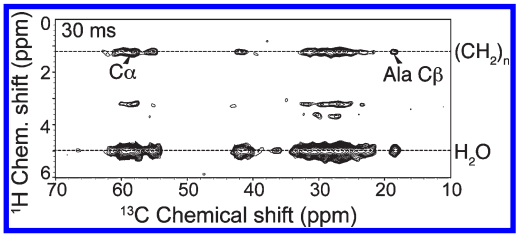

FIGURE 5: ^{1}H−^{13}C 2D spectra of MSP1D1 in POPC Nanodiscs. The experimental spectrum was acquired on uniformly ^{13}C-, ^{15}N-labeled MSP1D1 at 15 °C. Spectra were recorded with a 1 ms T_2 filter, a 0.4 ms ^{1}H−^{13}C contact time, and a 30 ms ^{1}H−^{1}H mixing time. The spectrum was processed with back linear prediction, 100 Hz net line broadening in the direct dimension, and 80 Hz in the indirect dimension (Lorentzian-to-Gaussian apodization), and zero filled to 4096 (ω_2) × 16384 (ω_1) complex points before Fourier transformation. Data were acquired in ~7 h.

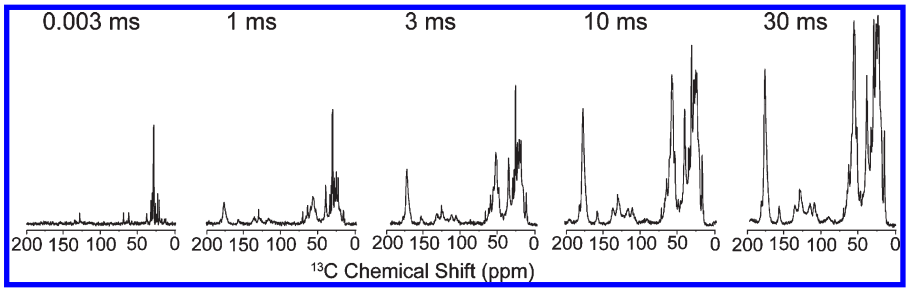

FIGURE 4: ^{13}C 1D spectra of MSP1D1 in POPC Nanodiscs. Spectra were recorded on uniformly ^{13}C-, ^{15}N-labeled MSP1D1 at 8 °C. ^{13}C 1D spectra were recorded with a 1 ms T_2 filter and a 0.4 ms HC contact time, where the ^{1}H−^{1}H mixing time was incremented and sequentially set to 3 μs, 1 ms, 3 ms, 10 ms, and 30 ms. The data were processed with 30 Hz Lorentzian-to-Gaussian line broadening.

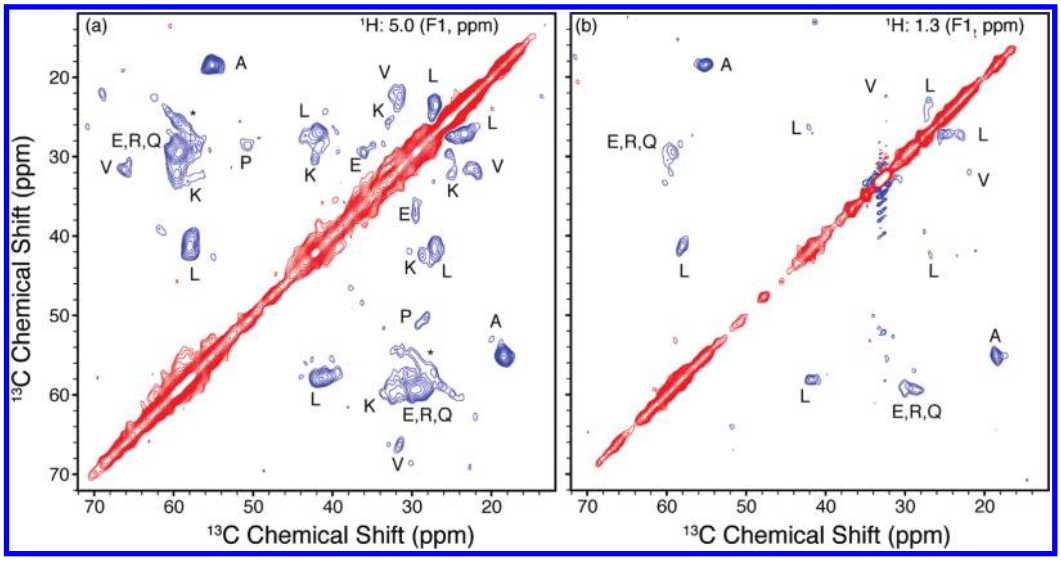

FIGURE 6: ^{1}H−^{13}C−^{13}C 3D spectrum of MSP1D1 in Nanodiscs. ^{1}H−^{13}C−^{13}C spectrum recorded at 600 MHz (^{1}H frequency) and a sample temperature of 8 °C in ~115 h. The T_2 filter time was set to 1 ms to eliminate protein ^{1}H polarization. A ^{1}H−^{1}H mixing time of 30 ms was used followed by ^{1}H−^{13}C cross-polarization. ^{13}C−^{13}C mixing with 12 ms of SPC-5 was used without the double quantum filter. Water (a) and lipid (b) ^{13}C−^{13}C planes are shown with peaks labeled by amino acid type (*87*). Positive contours are colored red and negative contours blue. The seeming artifact in the lipid plane is due to a strong signal originating from lipids correlated to themselves.

tentatively assigned by amino acid type. Clearly, a 3D spectrum is required to conduct more detailed analysis.

^{1}H−^{13}C−^{13}C 3D Spectrum for Identification of Lipid Interfaced MSP Residues by Amino Acid Type. MSP, like ApoA-I, has a repetitive amino acid sequence with several similar amphipathic α-helices. The ^{13}C chemical shifts are only partially resolved in two ^{13}C dimensions; however, this same uniform secondary structure enables us to readily identify the chemical shifts of specific amino acids (Ala, Leu, Val, Pro, and Lys) and classify the remaining signals into groups (e.g., Glu, Gln, and Arg). To separate the lipid and water correlations, we retained the ^{1}H dimension, while also digitizing the indirect ^{13}C dimension, resulting in a ^{1}H−^{13}C−^{13}C 3D experiment. In this case, we chose SPC-5 ^{13}C−^{13}C double quantum mixing (but without the coherence filter), because this was more sensitive under these experimental conditions. The short SPC-5 mixing time results in only one-bond ^{13}C−^{13}C cross-peaks, simplifying the spectral analysis and enabling the identification of several amino acid types without cancellation of signals due to multibond transfers.

Figure 6 shows the ^{13}C−^{13}C planes of the ^{1}H−^{13}C−^{13}C 3D spectrum at the water proton (a) (^{1}H of 5 ppm) and lipid proton (b) (^{1}H of 1.3 ppm) chemical shifts. The resolution in the proton dimension is sufficient to differentiate between the water plane and lipid acyl chain plane (~1 ppm). Resolving the protons of lipid acyl chains from the lipid terminal methyl group would be challenging with these experiments, although it is easily achieved in ^{1}H−^{13}C 2D experiments described above. Both strips show cross-peaks that can be confidently assigned by amino acid type, allowing further analysis. Both the water and lipid planes show peaks corresponding to uniquely resolved amino acid types Ala, Leu, and Val, as well as intensity grouped among Glu, Gln, and Arg; all of these shift patterns are consistent with helical secondary structure. In addition, the water plane (Figure 6a) shows correlations corresponding to Lys and Pro. The relative intensity of the cross-peaks within each plane, as well as the absolute intensity of each plane in total, varies depending on the source of polarization. The peaks in both ^{13}C−^{13}C planes were picked in NMRPipe (*72*) and integrated using the nlinLS package.

Table 1: Intensity Ratios for Water−Protein and Lipid−Protein Correlations

amino acid	MD ratio[a]	NMR ratio[b]	NMR confidence[c]
A	3.7	2.4	0.3
EQR	8.3	3.7	0.6
K	6.8	3.7	0.8
L	3.0	3.1	0.4
V	1.2	2.4	0.5

[a]Calculated as the ratio of CB carbons within 4.0 Å of water or lipid over the last 0.75 ns of a 4.5 ns MD simulation of MSP Nanodiscs. [b]Calculated as the ratio of ^{13}C−^{13}C cross-peaks to lipid and water in the ^{1}H−^{13}C−^{13}C 3D spectrum. [c]Calculated as $\Delta = [(1/I_{water})^2 + (1/I_{lipid})^2]^{1/2}$, where I_{water} and I_{lipid} are the signal:noise ratios of the water and lipid peaks, respectively, used in the calculation.

These intensities provide a semiquantitative assessment of which amino acids are in the proximity of water and/or lipid. We then compared these results with those from a 4.5 ns MD simulation of MSP1D1 in Nanodiscs (*24*).

It should be noted that the Nanodiscs used in the MD simulations were composed of DPPC lipids in a lipid gel phase, but given the time scales simulated (< 10 ns), lipid diffusion is not actually observed within the simulations. The simulations do, however, provide sufficient time for the lipids to relax around the amphipathic helices of MSP, allowing for determination of which amino acid residues are in contact with the lipids. As the comparisons with the NMR measurements are only looking at the matching of hydrophobic amino acids with lipid acyl chains, the difference in lipid type in the experimental data and the MD simulations is not expected to affect the resulting analysis.

We analyzed the MD trajectories according to the following strategy. The majority of cross-peaks in the 2D ^{13}C−^{13}C planes are CA−CB or CB−CG cross-peaks, consistent with the expectation that polarization is transferred from lipid or water to the amino acid side chain. We averaged the distance (over the final 0.75 ns of the MD trajectory) from each CB to the closest lipid acyl chain or water molecule. Because the absolute intensity of each plane depends upon a number of factors that cannot be

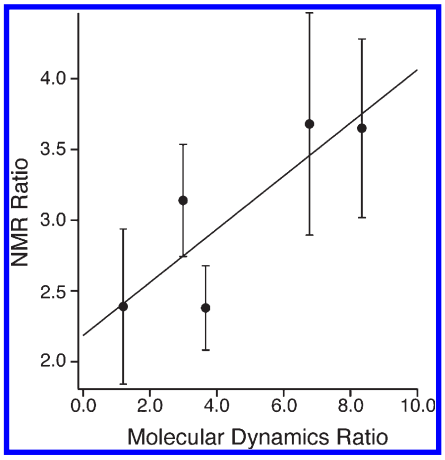

FIGURE 7: Plot of water:lipid ratios determined by NMR and molecular dynamics. Ratio of CB carbons in MSP within 4.0 Å of a water molecule to the ratio of CB carbons within 4.0 Å of lipid plotted vs the ratio of cross peak intensities for the same residues at the water and lipid ^{1}H frequencies in the ^{1}H−^{13}C−^{13}C 3D spectrum. MD ratios are the average number of CB atoms for a given residue within 4.0 Å of lipid or water averaged over two MSP molecules for the last 0.75 ns of a 4.5 ns MD simulation (*24*). NMR ratios were calculated using integrated peak intensities for ^{13}C−^{13}C cross-peaks corresponding to the same residues appearing at both the lipid and water ^{1}H frequency in the ^{1}H−^{13}C−^{13}C 3D spectrum. Error bars for the NMR ratio were calculated using the signal-to-noise of the peaks in the 3D spectrum using the method of Mani et al. (*63*). The linear best fit line is plotted. The NMR ratio is scaled due to different ^{1}H T_2 values as well as differences in total initial polarization.

predicted from theory (absolute polarization, range of T_2 values, diffusion rates, etc.), we normalized the data to the common ratio of intensities. For the MD simulations, this was the *W*:*L* ratio, where *W* is the number of residues within 4.0 Å of water and *L* is the number of residues within 4.0 Å of lipids. We then calculated the observed ratio of NMR signal intensity for *W* and *L*, corresponding to the ^{13}C−^{13}C cross-peaks occurring in the respective planes (~5.0 ppm for *W* and 1.3 ppm for *L*). These results are summarized in Table 1 and Figure 7. Figure 7 shows a graph of the *W*:*L* ratios in the NMR and MD experiments, along with a line of best fit. Error bars for the NMR data were calculated using the signal-to-noise ratio of the peaks in the same manner as Mani et al. (*63*), in the case of Leu, averaging the multiple observed cross-peaks. As expected, the data show a higher *W*:*L* ratio for charged and polar residues (Glu, Gln, Arg, and Lys) than for hydrophobic residues (Ala, Leu, and Val) in both cases. Indeed, for Lys and Glu, the lipid correlations were weak, but still observable. This is consistent with previously published results from modeling (*85*) and the published X-ray structure of truncated apo A-I (*86*), where a number of charged residues can be found associated with the lipid interface.

These results with MSP1D1 in Nanodiscs demonstrate the potential of the ^{1}H−^{13}C−^{13}C pulse sequence for obtaining information about the membrane protein topology and lipid−protein interfaces. The information that can be obtained in the case of MSP is limited by the large portion of the protein interacting with the lipid bilayer (approximately one-third of 211 residues), and the degeneracy in the chemical shift distribution due to all amino acids being present in a helical secondary structure. More qualitative information can certainly be obtained from experiments like these in combination with amino acid type-specific isotope labeling schemes of the protein of interest, and more quantitative information if site-specific assignments for the protein are available.

CONCLUSIONS

In this work, we have demonstrated a new sample preparation method for POPC Nanodiscs and applied SSNMR in examining a membrane−protein interface. SSNMR was used to assess the phase transition behavior of the lipid bilayer in a Nanodisc and confirm that under the sample preparation conditions POPC Nanodiscs exhibited the expected gel to liquid crystalline phase transition characteristic of POPC lipid bilayers. Using MSP1D1 Nanodiscs, we demonstrated that the ^{1}H−^{13}C−^{13}C 3D pulse sequence provides qualitative information about the protein residues at the lipid−protein boundary. The experimental information was compared to results of MD simulation of Nanodiscs, and it was found that the experimental results are consistent with the predicted lipid−protein interface from the MD simulations in amino acid type and number of residues in the interface. The study demonstrates the potential for use of the Nanodisc platform in combination with presented proton spin diffusion experiments in the examination of lipid−protein interfaces and membrane topology for embedded membrane proteins.

ACKNOWLEDGMENT

We thank Dr. Ying Li for her involvement in early stages of the development and application of the SSNMR experiment and John M. Boettcher, Rebecca L. Davis-Harrison, and Yelena V. Grinkova for discussions about sample preparation.

SUPPORTING INFORMATION AVAILABLE

Normalized gel filtration chromatograms of POPC Nanodiscs before and after lyophilization and rehydration (Figure S1) and ratios of intensities for the water−protein and lipid−protein correlations in the water plane of the 3D experiment (Table S1). This material is available free of charge via the Internet at http://pubs.acs.org.

REFERENCES

1. Zwaal, R. F., Comfurius, P., and Bevers, E. M. (1998) Lipid-protein interactions in blood coagulation. *Biochim. Biophys. Acta 1376*, 433–453.
2. Shaw, A. W., Pureza, V. S., Sligar, S. G., and Morrissey, J. H. (2007) The local phospholipid environment modulates the activation of blood clotting. *J. Biol. Chem. 282*, 6556–6563.
3. Yun, C. H., Ahn, T., and Guengerich, F. P. (1998) Conformational change and activation of cytochrome P450 2B1 induced by salt and phospholipid. *Arch. Biochem. Biophys. 356*, 229–238.
4. Kim, K. H., Ahn, T., and Yun, C. H. (2003) Membrane properties induced by anionic phospholipids and phosphatidylethanolamine are critical for the membrane binding and catalytic activity of human cytochrome P450 3A4. *Biochemistry 42*, 15377–15387.
5. Ahn, T., Guengerich, F. P., and Yun, C. H. (1998) Membrane insertion of cytochrome P450 1A2 promoted by anionic phospholipids. *Biochemistry 37*, 12860–12866.
6. Chini, B., and Parenti, M. (2009) G-protein coupled receptors, cholesterol and palmitoylation: Facts about fats. *J. Mol. Endocrinol. 42*, 9.
7. Bernier, L. P., Ase, A. R., Chevallier, S., Blais, D., Zhao, Q., Boue-Grabot, E., Logothetis, D., and Seguela, P. (2008) Phosphoinositides regulate P2X4 ATP-gated channels through direct interactions. *J. Neurosci. 28*, 12938–12945.
8. Thomas, A. M., and Tinker, A. (2008) Determination of phosphoinositide binding to K^+ channel subunits using a protein-lipid overlay assay. *Methods Mol. Biol. 491*, 103–111.
9. Mani, R., Buffy, J. J., Waring, A. J., Lehrer, R. I., and Hong, M. (2004) Solid-state NMR investigation of the selective disruption of lipid membranes by protegrin-1. *Biochemistry 43*, 13839–13848.
10. Matsuzaki, K., Murase, O., and Miyajima, K. (1995) Kinetics of pore formation by an antimicrobial peptide, magainin 2, in phospholipid bilayers. *Biochemistry 34*, 12553–12559.

11. Prenner, E. J., Lewis, R. N., and McElhaney, R. N. (1999) The interaction of the antimicrobial peptide gramicidin S with lipid bilayer model and biological membranes. *Biochim. Biophys. Acta 1462*, 201–221.
12. Morrissey, J. H., Pureza, V., Davis-Harrison, R. L., Sligar, S. G., Ohkubo, Y. Z., and Tajkhorshid, E. (2008) Blood clotting reactions on nanoscale phospholipid bilayers. *Thromb. Res. 122* (Suppl. 1), S23–S26.
13. Vinogradova, O., Sonnichsen, F., and Sanders, C. R. (1998) On choosing a detergent for solution NMR studies of membrane proteins. *J. Biomol. NMR 11*, 381–386.
14. Sorgen, P. L., Cahill, S. M., Krueger-Koplin, R. D., Krueger-Koplin, S. T., Schenck, C. C., and Girvin, M. E. (2002) Structure of the *Rhodobacter sphaeroides* light-harvesting 1 β subunit in detergent micelles. *Biochemistry 41*, 31–41.
15. Bayburt, T. H., Carlson, J. W., and Sligar, S. G. (1998) Reconstitution and imaging of a membrane protein in a nanometer-size phospholipid bilayer. *J. Struct. Biol. 123*, 37–44.
16. Bayburt, T. H., Grinkova, Y. V., and Sligar, S. G. (2002) Self-assembly of discoidal phospholipid bilayer nanoparticles with membrane scaffold proteins. *Nano Lett. 2*, 853–856.
17. Baas, B. J., Denisov, I. G., and Sligar, S. G. (2004) Homotropic cooperativity of monomeric cytochrome P450 3A4 in a nanoscale native bilayer environment. *Arch. Biochem. Biophys. 430*, 218–228.
18. Denisov, I. G., Grinkova, Y. V., Lazarides, A. A., and Sligar, S. G. (2004) Directed self-assembly of monodisperse phospholipid bilayer Nanodiscs with controlled size. *J. Am. Chem. Soc. 126*, 3477–3487.
19. Shaw, A. W., McLean, M. A., and Sligar, S. G. (2004) Phospholipid phase transitions in homogeneous nanometer scale bilayer discs. *FEBS Lett. 556*, 260–264.
20. Denisov, I. G., McLean, M. A., Shaw, A. W., Grinkova, Y. V., and Sligar, S. G. (2005) Thermotropic phase transition in soluble nanoscale lipid bilayers. *J. Phys. Chem. B 109*, 15580–15588.
21. Bayburt, T. H., Grinkova, Y. V., and Sligar, S. G. (2006) Assembly of single bacteriorhodopsin trimers in bilayer nanodiscs. *Arch. Biochem. Biophys. 450*, 215–222.
22. Nath, A., Atkins, W. M., and Sligar, S. G. (2007) Applications of phospholipid bilayer nanodiscs in the study of membranes and membrane proteins. *Biochemistry 46*, 2059–2069.
23. Bayburt, T. H., Leitz, A. J., Xie, G., Oprian, D. D., and Sligar, S. G. (2007) Transducin activation by nanoscale lipid bilayers containing one and two rhodopsins. *J. Biol. Chem. 282*, 14875–14881.
24. Shih, A. Y., Denisov, I. G., Phillips, J. C., Sligar, S. G., and Schulten, K. (2005) Molecular dynamics simulations of discoidal bilayers assembled from truncated human lipoproteins. *Biophys. J. 88*, 548–556.
25. Shih, A. Y., Freddolino, P. L., Sligar, S. G., and Schulten, K. (2007) Disassembly of nanodiscs with cholate. *Nano Lett. 7*, 1692–1696.
26. Denisov, I. G., Baas, B. J., Grinkova, Y. V., and Sligar, S. G. (2007) Cooperativity in cytochrome P450 3A4: Linkages in substrate binding, spin state, uncoupling, and product formation. *J. Biol. Chem. 282*, 7066–7076.
27. Civjan, N. R., Bayburt, T. H., Schuler, M. A., and Sligar, S. G. (2003) Direct solubilization of heterologously expressed membrane proteins by incorporation into nanoscale lipid bilayers. *BioTechniques 35* (556−560), 562–553.
28. Nath, A., Grinkova, Y. V., Sligar, S. G., and Atkins, W. M. (2007) Ligand binding to cytochrome P450 3A4 in phospholipid bilayer nanodiscs: The effect of model membranes. *J. Biol. Chem. 282*, 28309–28320.
29. Alami, M., Dalal, K., Lelj-Garolla, B., Sligar, S. G., and Duong, F. (2007) Nanodiscs unravel the interaction between the SecYEG channel and its cytosolic partner SecA. *EMBO J. 26*, 1995–2004.
30. Leitz, A. J., Bayburt, T. H., Barnakov, A. N., Springer, B. A., and Sligar, S. G. (2006) Functional reconstitution of β2-adrenergic receptors utilizing self-assembling Nanodisc technology. *BioTechniques 40*, 601–612.
31. Boldog, T., Grimme, S., Li, M., Sligar, S. G., and Hazelbauer, G. L. (2006) Nanodiscs separate chemoreceptor oligomeric states and reveal their signaling properties. *Proc. Natl. Acad. Sci. U.S.A. 103*, 11509–11514.
32. Li, Y., Kijac, A. Z., Sligar, S. G., and Rienstra, C. M. (2006) Structural analysis of nanoscale self-assembled discoidal lipid bilayers by solid-state NMR spectroscopy. *Biophys. J. 91*, 3819–3828.
33. Kijac, A. Z., Li, Y., Sligar, S. G., and Rienstra, C. M. (2007) Magic-angle spinning solid-state NMR spectroscopy of nanodisc-embedded human CYP3A4. *Biochemistry 46*, 13696–13703.
34. Lyukmanova, E. N., Shenkarev, Z. O., Paramonov, A. S., Sobol, A. G., Ovchinnikova, T. V., Chupin, V. V., Kirpichnikov, M. P., Blommers, M. J. J., and Arseniev, A. S. (2008) Lipid-protein nanoscale bilayers: A versatile medium for NMR investigations of membrane proteins and membrane-active peptides. *J. Am. Chem. Soc. 130*, 2140.
35. Lyukmanova, E. N., Shenkarev, Z. O., Ovchinnikova, T. V., Chupin, V. V., Blommers, M. J. J., and Arseniev, A. S. (2008) Reconstituted high density lipoprotein particles: A promising medium for high-resolution NMR investigations of membrane proteins and membrane-active peptides. *FEBS J. 275*, 171.
36. Gluck, J. M., Wittlich, M., Feuerstein, S., Hoffmann, S., Willbold, D., and Koenig, B. W. (2009) Integral Membrane Proteins in Nanodiscs Can Be Studied by Solution NMR Spectroscopy. *J. Am. Chem. Soc. 131*, 12060.
37. Boldog, T., Grimme, S., Li, M., Sligar, S. G., and Hazelbauer, G. L. (2006) Nanodiscs separate chemoreceptor oligomeric states and reveal their signaling properties. *Proc. Natl. Acad. Sci. U.S.A. 103*, 11509–11514.
38. Shaw, A. W., Pureza, V. S., Sligar, S. G., and Morrissey, J. H. (2007) The local phospholipid environment modulates the activation of blood clotting. *J. Biol. Chem. 282*, 6556–6563.
39. Baas, B. J., Denisov, I. G., and Sligar, S. G. (2004) Homotropic cooperativity of monomeric cytochrome P450 3A4 in a nanoscale native bilayer environment. *Arch. Biochem. Biophys. 430*, 218–228.
40. Denisov, I. G., Grinkova, Y. V., Baas, B. J., and Sligar, S. G. (2006) The ferrous-dioxygen intermediate in human cytochrome P450 3A4. Substrate dependence of formation and decay kinetics. *J. Biol. Chem. 281*, 23313–23318.
41. Davydov, D. R., Fernando, H., Baas, B. J., Sligar, S. G., and Halpert, J. R. (2005) Kinetics of dithionite-dependent reduction of cytochrome P450 3A4: Heterogeneity of the enzyme caused by its oligomerization. *Biochemistry 44*, 13902–13913.
42. Bayburt, T. H., Grinkova, Y. V., and Sligar, S. G. (2006) Assembly of single bacteriorhodopsin trimers in bilayer nanodiscs. *Arch. Biochem. Biophys. 450*, 215–222.
43. Bayburt, T. H., Leitz, A. J., Xie, G., Oprian, D. D., and Sligar, S. G. (2007) Transducin activation by nanoscale lipid bilayers containing one and two rhodopsins. *J. Biol. Chem. 282*, 14875–14881.
44. Alami, M., Dalal, K., Lelj-Garolla, B., Sligar, S. G., and Duong, F. (2007) Nanodiscs unravel the interaction between the SecYEG channel and its cytosolic partner SecA. *EMBO J. 26*, 1995–2004.
45. Dalal, K., Nguyen, N., Alami, M., Tan, J., Moraes, T. F., Lee, W. C., Maurus, R., Sligar, S. S., Brayer, G. D., and Duong, F. (2009) Structure, Binding, and Activity of Syd, a SecY-interacting Protein. *J. Biol. Chem. 284*, 7897–7902.
46. Duan, H., Civjan, N. R., Sligar, S. G., and Schuler, M. A. (2004) Co-incorporation of heterologously expressed *Arabidopsis* cytochrome P450 and P450 reductase into soluble nanoscale lipid bilayers. *Arch. Biochem. Biophys. 424*, 141–153.
47. Denisov, I. G., Baas, B. J., Grinkova, Y. V., and Sligar, S. G. (2007) Cooperativity in cytochrome P450 3A4: Linkages in substrate binding, spin state, uncoupling, and product formation. *J. Biol. Chem. 282*, 7066–7076.
48. Bayburt, T. H., and Sligar, S. G. (2010) Membrane protein assembly into Nanodiscs. *FEBS Lett. 584*, 1721–1727.
49. Borch, J., and Hamann, T. (2009) The nanodisc: A novel tool for membrane protein studies. *Biol. Chem. 390*, 805–814.
50. Li, Y., Berthold, D. A., Gennis, R. B., and Rienstra, C. M. (2008) Chemical shift assignment of the transmembrane helices of DsbB, a 20-kDa integral membrane enzyme, by 3D magic-angle spinning NMR spectroscopy. *Protein Sci. 17*, 199–204.
51. Frericks, H. L., Zhou, D. H., Yap, L. L., Gennis, R. B., and Rienstra, C. M. (2006) Magic-angle spinning solid-state NMR of a 144 kDa membrane protein complex: *E. coli* cytochrome bo_3 oxidase. *J. Biomol. NMR 36*, 55–71.
52. Shi, L., Ahmed, M. A., Zhang, W., Whited, G., Brown, L. S., and Ladizhansky, V. (2009) Three-dimensional solid-state NMR study of a seven-helical integral membrane proton pump: Structural insights. *J. Mol. Biol. 386*, 1078–1093.
53. Etzkorn, M., Martell, S., Andronesi, O. C., Seidel, K., Engelhard, M., and Baldus, M. (2007) Secondary structure, dynamics, and topology of a seven-helix receptor in native membranes, studied by solid-state NMR spectroscopy. *Angew. Chem., Int. Ed. 46*, 459–462.
54. Wasmer, C., Lange, A., Van Melckebeke, H., Siemer, A. B., Riek, R., and Meier, B. H. (2008) Amyloid fibrils of the HET-s(218−289) prion form a β solenoid with a triangular hydrophobic core. *Science 319*, 1523–1526.
55. Petkova, A. T., Leapman, R. D., Guo, Z., Yau, W. M., Mattson, M. P., and Tycko, R. (2005) Self-propagating, molecular-level polymorphism in Alzheimer's β-amyloid fibrils. *Science 307*, 262–265.

56. Castellani, F., van Rossum, B., Diehl, A., Schubert, M., Rehbein, K., and Oschkinat, H. (2002) Structure of a protein determined by solid-state magic-angle-spinning NMR spectroscopy. *Nature 420*, 98–102.
57. Park, S. H., Mrse, A. A., Nevzorov, A. A., Mesleh, M. F., Oblatt-Montal, M., Montal, M., and Opella, S. J. (2003) Three-dimensional structure of the channel-forming trans-membrane domain of virus protein "u" (Vpu) from HIV-1. *J. Mol. Biol. 333*, 409–424.
58. Kamihira, M., Vosegaard, T., Mason, A. J., Straus, S. K., Nielsen, N. C., and Watts, A. (2005) Structural and orientational constraints of bacteriorhodopsin in purple membranes determined by oriented-sample solid-state NMR spectroscopy. *J. Struct. Biol. 149*, 7–16.
59. Park, S. H., Prytulla, S., De Angelis, A. A., Brown, J. M., Kiefer, H., and Opella, S. J. (2006) High-resolution NMR spectroscopy of a GPCR in aligned bicelles. *J. Am. Chem. Soc. 128*, 7402–7403.
60. Liu, W., Crocker, E., Constantinescu, S. N., and Smith, S. O. (2005) Helix packing and orientation in the transmembrane dimer of gp55-P of the spleen focus forming virus. *Biophys. J. 89*, 1194–1202.
61. Liu, W., Crocker, E., Siminovitch, D. J., and Smith, S. O. (2003) Role of side-chain conformational entropy in transmembrane helix dimerization of glycophorin A. *Biophys. J. 84*, 1263–1271.
62. Toke, O., O'Connor, R. D., Weldeghiorghis, T. K., Maloy, W. L., Glaser, R. W., Ulrich, A. S., and Schaefer, J. (2004) Structure of $(KIAGKIA)_3$ aggregates in phospholipid bilayers by solid-state NMR. *Biophys. J. 87*, 675–687.
63. Mani, R., Cady, S. D., Tang, M., Waring, A. J., Lehrer, R. I., and Hong, M. (2006) Membrane-dependent oligomeric structure and pore formation of a β-hairpin antimicrobial peptide in lipid bilayers from solid-state NMR. *Proc. Natl. Acad. Sci. U.S.A. 103*, 16242–16247.
64. Huster, D., Yao, X., and Hong, M. (2002) Membrane protein topology probed by ^{1}H spin diffusion from lipids using solid-state NMR spectroscopy. *J. Am. Chem. Soc. 124*, 874–883.
65. Buffy, J. J., Hong, T., Yamaguchi, S., Waring, A. J., Lehrer, R. I., and Hong, M. (2003) Solid-state NMR investigation of the depth of insertion of protegrin-1 in lipid bilayers using paramagnetic Mn^{2+}. *Biophys. J. 85*, 2363–2373.
66. Prosser, R. S., Luchette, P. A., and Westerman, P. W. (2000) Using O_2 to probe membrane immersion depth by ^{19}F NMR. *Proc. Natl. Acad. Sci. U.S.A. 97*, 9967–9971.
67. Hong, M. (2006) Oligomeric structure, dynamics, and orientation of membrane proteins from solid-state NMR. *Structure 14*, 1731–1740.
68. Kumashiro, K. K., Schmidt-Rohr, K., Murphy, O. J., Ouellette, K. L., Cramer, W. A., and Thompson, L. K. (1998) A novel tool for probing membrane protein structure: Solid-state NMR with proton spin diffusion and X-nucleus detection. *J. Am. Chem. Soc. 120*, 5043–5051.
69. Franks, W. T., Zhou, D. H., Wylie, B. J., Money, B. G., Graesser, D. T., Frericks, H. L., Sahota, G., and Rienstra, C. M. (2005) Magic-angle spinning solid-state NMR spectroscopy of the β1 immunoglobulin binding domain of protein G (GB1): ^{15}N and ^{13}C chemical shift assignments and conformational analysis. *J. Am. Chem. Soc. 127*, 12291–12305.
70. Hediger, S., Meier, B. H., Kurur, N. D., Bodenhausen, G., and Ernst, R. R. (1994) NMR cross-polarization by adiabatic passage through the Hartmann-Hahn condition (APHH). *Chem. Phys. Lett. 223*, 283–288.
71. Bennett, A. E., Rienstra, C. M., Auger, M., Lakshmi, K. V., and Griffin, R. G. (1995) Heteronuclear decoupling in rotating solids. *J. Chem. Phys. 103*, 6951–6958.
72. Delaglio, F., Grzesiek, S., Vuister, G. W., Zhu, G., Pfeifer, J., and Bax, A. (1995) NMRPipe: A multidimensional spectral processing system based on Unix pipes. *J. Biomol. NMR 6*, 277–293.
73. Morcombe, C. R., and Zilm, K. W. (2003) Chemical shift referencing in MAS solid state NMR. *J. Magn. Reson. 162*, 479–486.
74. Humphrey, W., Dalke, A., and Schulten, K. (1996) VMD: Visual molecular dynamics. *J. Mol. Graphics 14* (33−38), 27–38.
75. Stringer, J. A., Bronnimann, C. E., Mullen, C. G., Zhou, D. H., Stellfox, S. A., Li, Y., Williams, E. H., and Rienstra, C. M. (2005) Reduction of RF-induced sample heating with a scroll coil resonator structure for solid-state NMR probes. *J. Magn. Reson. 173*, 40–48.
76. Golovina, E. A., Golovin, A. V., Hoekstra, F. A., and Faller, R. (2009) Water Replacement Hypothesis in Atomic Detail—Factors Determining the Structure of Dehydrated Bilayer Stacks. *Biophys. J. 97*, 490–499.
77. Tsvetkova, N. M., Phillips, B. L., Crowe, L. M., Crowe, J. H., and Risbud, S. H. (1998) Effect of sugars on headgroup mobility in freeze-dried dipalmitoylphosphatidylcholine bilayers: Solid-state ^{31}P NMR and FTIR studies. *Biophys. J. 75*, 2947–2955.
78. Crowe, L. M., and Crowe, J. H. (1988) Dry Dipalmitoylphosphatidylcholine and Trehalose Revisited. *Biophys. J. 53*, A127.
79. Ammann, C., Meier, P., and Merbach, A. E. (1982) A Simple Multinuclear NMR Thermometer. *J. Magn. Reson. 46*, 319–321.
80. Koster, K. L., Webb, M. S., Bryant, G., and Lynch, D. V. (1994) Interactions between Soluble Sugars and Popc (1-Palmitoyl-2-Oleoylphosphatidylcholine) during Dehydration: Vitrification of Sugars Alters the Phase-Behavior of the Phospholipid. *Biochim. Biophys. Acta 1193*, 143–150.
81. Denisov, I. G., McLean, M. A., Shaw, A. W., Grinkova, Y. V., and Sligar, S. G. (2005) Thermotropic phase transition in soluble nanoscale lipid bilayers. *J. Phys. Chem. B 109*, 15580–15588.
82. Shaw, A. W., McLean, M. A., and Sligar, S. G. (2004) Phospholipid phase transitions in homogeneous nanometer scale bilayer discs. *FEBS Lett. 556*, 260–264.
83. Hohwy, M., Rienstra, C. M., Jaroniec, C. P., and Griffin, R. G. (1999) Fivefold symmetric homonuclear dipolar recoupling in rotating solids: Application to double quantum spectroscopy. *J. Chem. Phys. 110*, 7983–7992.
84. Forbes, J., Husted, C., and Oldfield, E. (1988) High-Field, High-Resolution Proton Magic-Angle Sample-Spinning Nuclear Magnetic-Resonance Spectroscopic Studies of Gel and Liquid-Crystalline Lipid Bilayers and the Effects of Cholesterol. *J. Am. Chem. Soc. 110*, 1059–1065.
85. Segrest, J. P., Jones, M. K., Klon, A. E., Sheldahl, C. J., Hellinger, M., De Loof, H., and Harvey, S. C. (1999) A detailed molecular belt model for apolipoprotein A-I in discoidal high density lipoprotein. *J. Biol. Chem. 274*, 31755–31758.
86. Borhani, D. W., Rogers, D. P., Engler, J. A., and Brouillette, C. G. (1997) Crystal structure of truncated human apolipoprotein A-I suggests a lipid-bound conformation. *Proc. Natl. Acad. Sci. U.S.A. 94*, 12291–12296.
87. Zhang, H., Neal, S., and Wishart, D. S. (2003) RefDB: A database of uniformly referenced protein chemical shifts. *J. Biomol. NMR 25*, 173–195.